Electronic Supplementary Material (ESI) for Dalton Transactions.

Supporting information

Synthesis of a miniaturized [FeFe] hydrogenase model system

Charlène Esmieu,[a] Meiyuan Guo,[b] Holly Redman, [a] Marcus Lundberg [b] and Gustav Berggren[a,*]

a) Molecular Biomimetics, Department of Chemistry – Ångström Laboratory, Uppsala University, 75120 Uppsala, Sweden; gustav.berggren@kemi.uu.se
b) Theoretical Chemistry, Department of Chemistry – Ångström Laboratory, Uppsala University, 75120 Uppsala, Sweden; marcus.lundberg@kemi.uu.se

Table of Contents

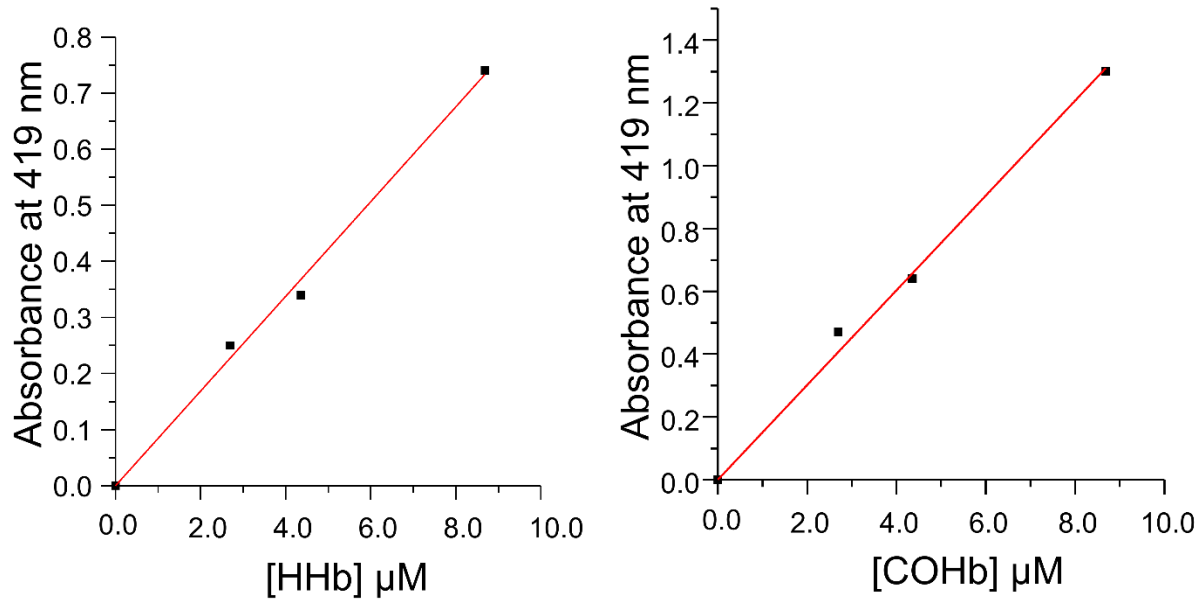

Figure S1. Determination of the molar absorptivity at 419 nm for the species HHb and CO-Hb. HHb has a high affinity for CO and the formation of CO-Hb results in a shift of the Soret band from 430 nm to 419 nm. CO-Hb (right) was generated by flushing stock solutions of HHb (left) with CO gas, and the ε_{419} for the different species was determined from the slope of the curve.

$\varepsilon_{419,\,HHb}$ = 84 000 L.mol^{-1}.cm^{-1} and $\varepsilon_{419,\,COHb}$ = 151 000 L.mol^{-1}.cm^{-1}

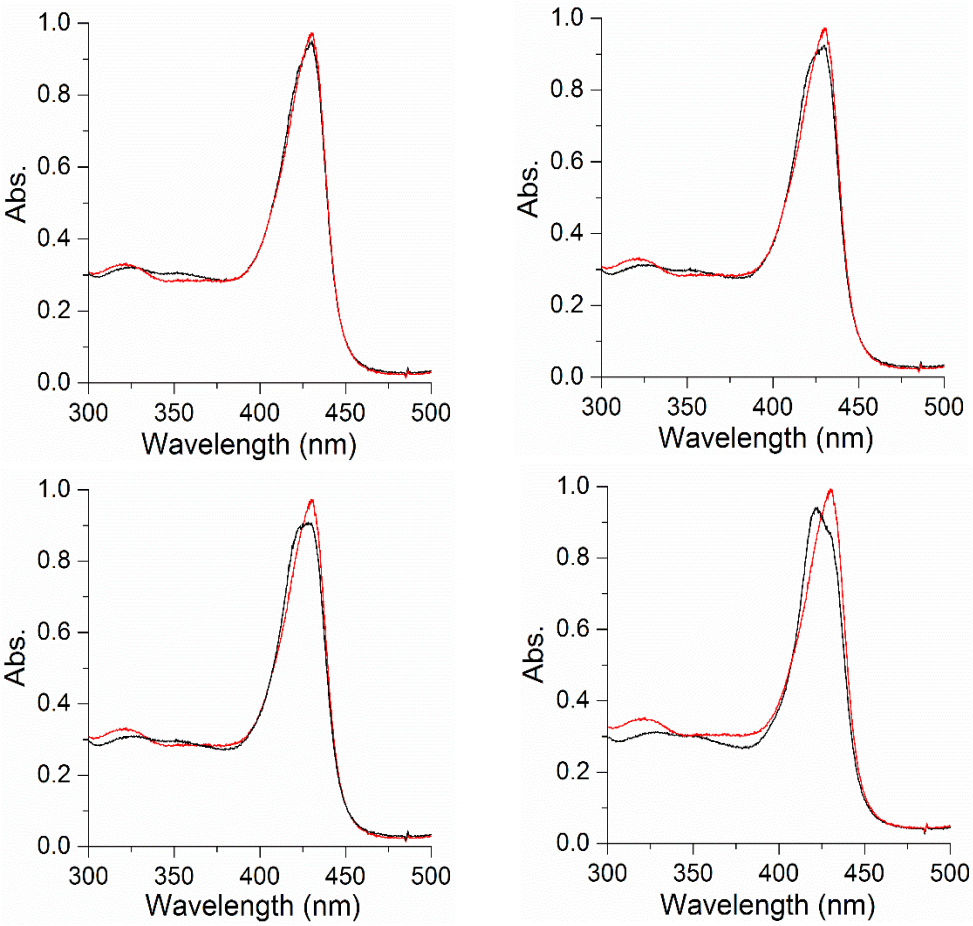

Figure S2. CO release from the reaction between $[4Fe4S]^+$ – FdM and **1** monitored by UV/Vis spectroscopy. A shift of the Soret band is observed within seconds after addition of deoxyhemoglobin to reaction mixtures containing stoichiometric amounts of $[4Fe4S]^+$ – FdM and **1** (change observed from red to black spectra). Concentrations of [4Fe4S] – FdM and **1**: 0.96 µM (top left), 1.4 µM (top right), 1.92 µM (bottom left) and 2.1 µM (bottom right), [dithionite] = 20 – 40 µM (20 eq. vs [4Fe4S] – FdM). The calculated CO release for each experiment: 0.70 µM, 1.0 µM, 1.2 µM, 1.4 µM in order of increasing [4Fe4S] – FdM concentration. All samples prepared in HEPES buffer (50 mM, pH 8), final volume 1 mL. Total concentration of hemoglobin 9 µM.

The released CO was quantified using equation 1 based on the absorbance observed at 419 nm.

$$[CO] = [HbCO] = (A_{419}-(\varepsilon_{419,\,HHb} \times [Hb]_T))/(\varepsilon_{419,\,COHb} - \varepsilon_{419,\,HHb}) \qquad (1)$$

$[Hb]_T$ = 9 µM = Total concentration of hemoglobin ([HHb] + [COHb])

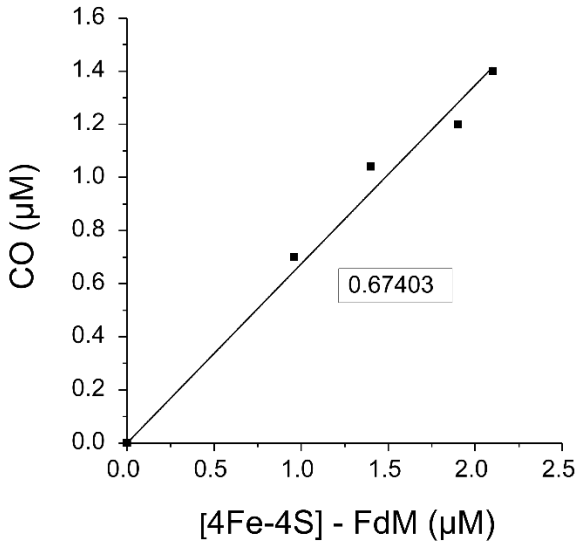

Figure S3. Observed CO release from the reaction between $[4Fe4S]^{+}$ – FdM and **1**, plotted as a function of initial [4Fe4S] – FdM concentration.

The linear fit indicate evolution of 0.67 mol CO per mol of [4Fe4S] – FdM, across the studied concentration interval.

Samples prepared as described in Figure S2.

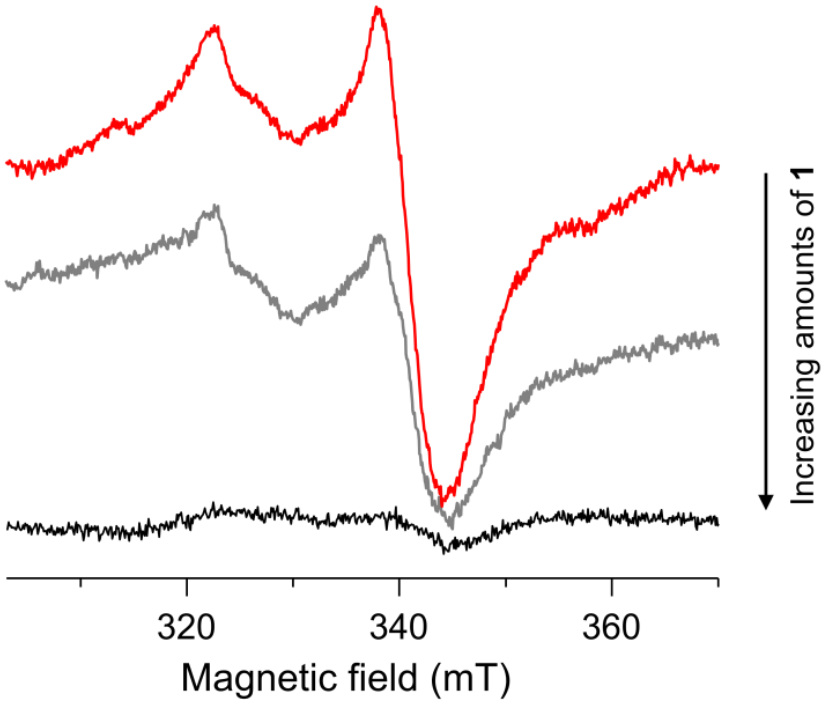

Figure S4. The reaction between **1** and $[4Fe4S]^{+}$-FdM monitored by X-band EPR spectroscopy. $[4Fe4S]^{+}$–FdM (30 μM) (**red spectrum**); $[4Fe4S]^{+}$–FdM (30 μM) + **1** (15 μM, 0.5 eq.) (**grey spectrum**); $[4Fe4S]^{+}$–FdM (30 μM) + **1** (30 μM, 1 eq.) (**black spectrum**). The addition of **1** results in disappearance of the rhombic EPR signal attributed to $[4Fe4S]^{+}$–FdM, with no new signal becoming discernible.

All samples prepared in HEPES buffer (50 mM, pH 8) and flash frozen after 30 minutes incubation time with **1**. Spectra recorded at 10K, microwave frequency 9.28 GHz, modulation amplitude: 10 G, microwave power: 1 mW.

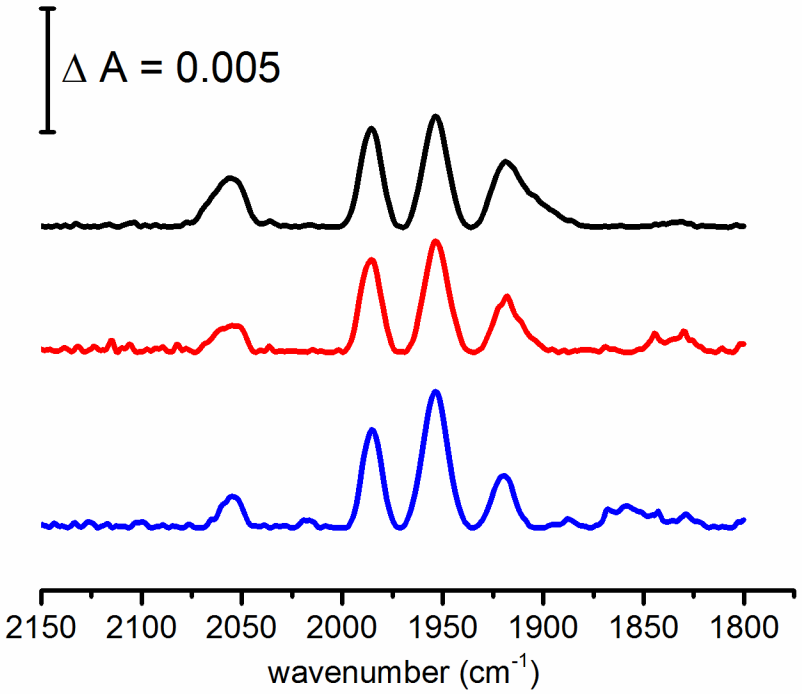

Figure S5. Stability of **1** in the presence of Fe, S^{2-} and dithionite monitored by FTIR spectroscopy. FTIR spectra recorded on a mixture of **1** (1.5 mM), Fe^{2+} (3 mM), Fe^{3+} (3 mM), S^{2-} (6 mM) without dithionite (**black spectrum**) and with dithionite (15 mM) added to the reaction mixture (**red spectrum**); FTIR spectrum of **1** (1.5 mM) (**blue spectrum**). All samples prepared in HEPES buffer (50 mM, pH 8).

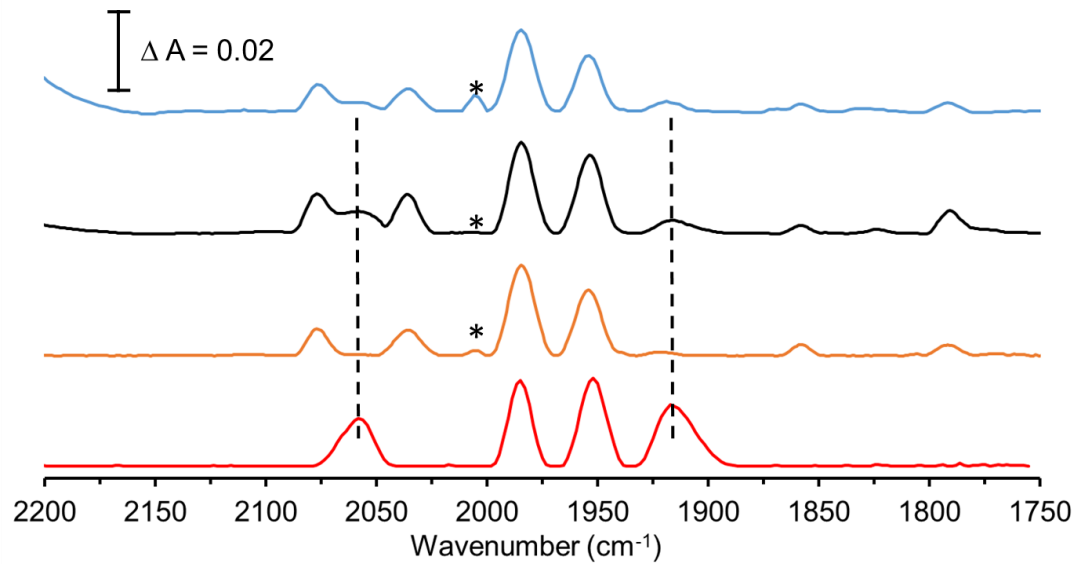

Figure S6. Removal of the 4th CO ligand by HHb monitored by FTIR spectroscopy. **Blue spectrum**: A solution of complex **2**, prepared as described in the main text [[4Fe4S]$^{+}$–FdM (800 μM) + **1** (400 μM, 0.5 eq.)]; **Black spectrum**: A solution of complex **2** prepared in an analogous fashion followed by addition of deoxyhemoglobin to remove labile CO ligands, resulting in the disappearance of the peak at 2005 cm^{-1} [[4Fe4S]$^{+}$–FdM (1000 μM) + **1** (500 μM, 0.5 eq.) + deoxyhemoglobin, HHb (2000 μM)]. The spectra of **1** in the presence of [4Fe4S]$^{2+}$-FdM (**Red spectrum**) and **2** (**Orange spectrum**) shown in Figure 3 of the main paper are redrawn for reference. The band attributed to the CO bound species indicated with an asterisk (*); The bands associated with unreacted **1** indicated with dashed vertical lines.

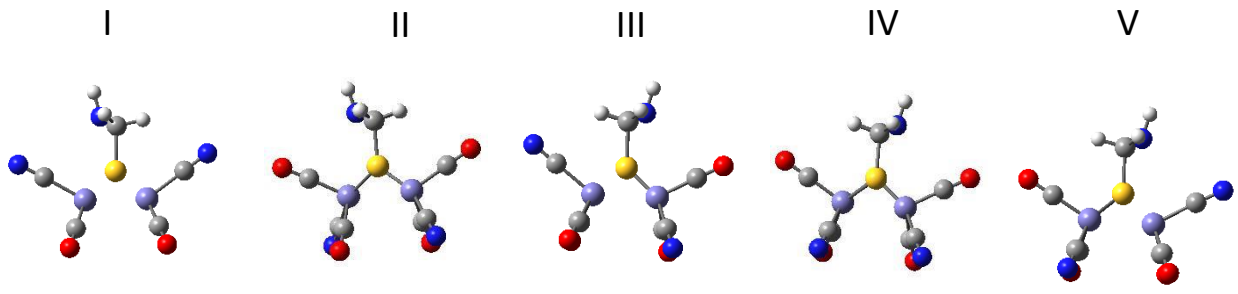

Figure S7. Five possible structures of $[Fe_2(adt)(CO)_4(CN)_2]^{2-}$ (**1**). Structures III and V have the same CN and CO ligand arrangement but different orientations of the bridging group. Colour coding: Fe - purple, Sulfur - yellow, O - red, N - blue, C - grey, hydrogen - white.

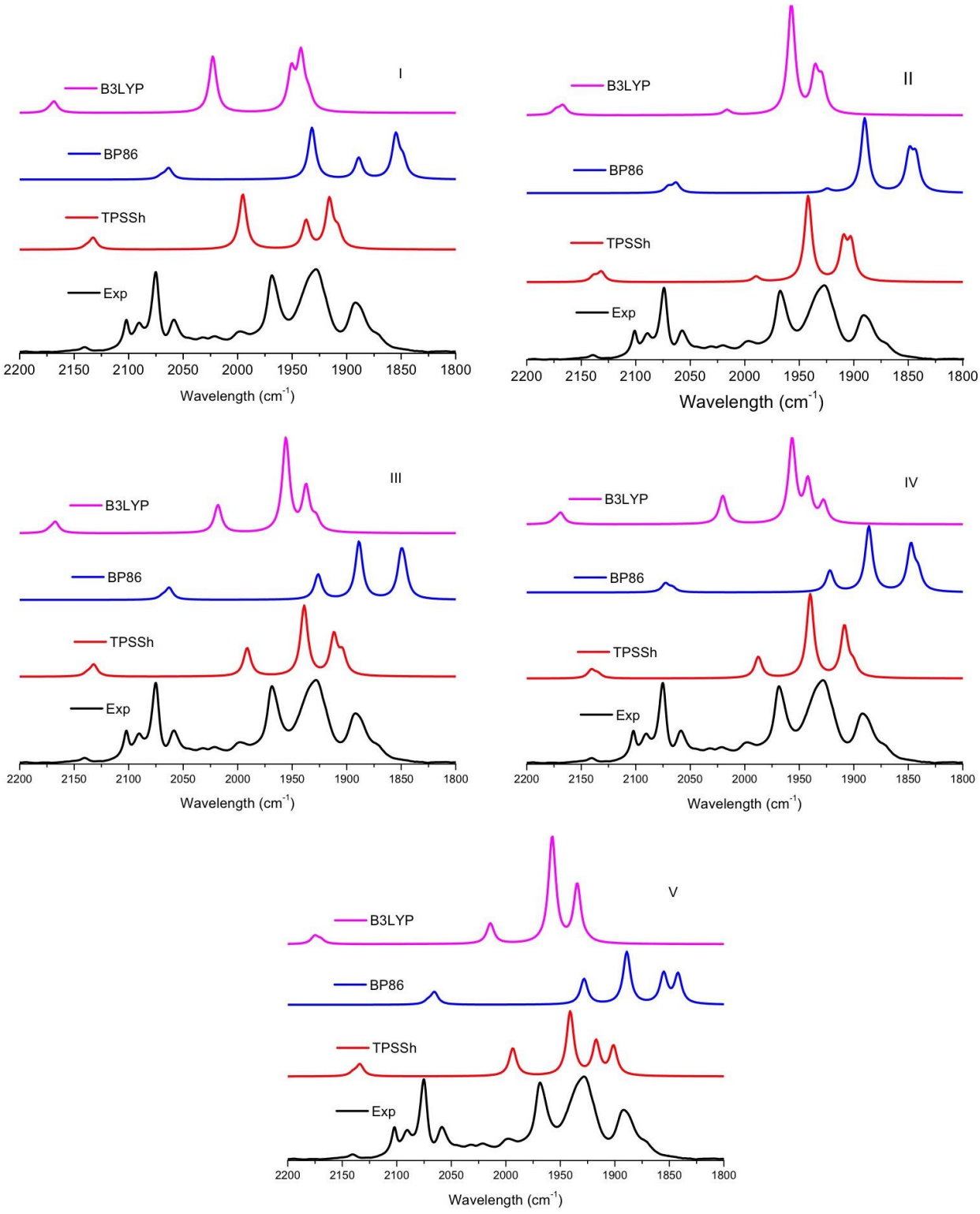

Figure S8. FTIR spectra of **1** from models **I-V** calculated with different DFT functionals using the TZVP basis set.

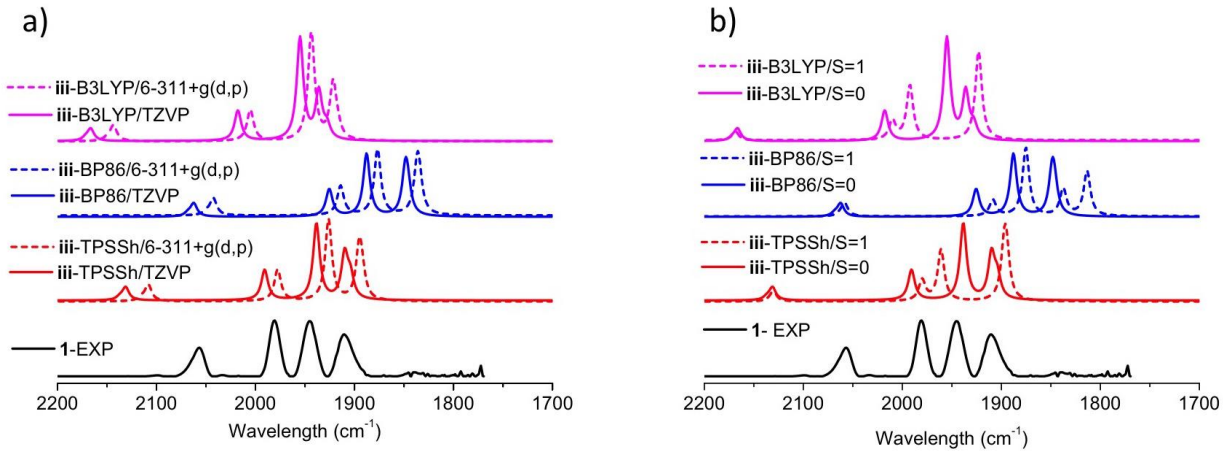

Figure S9. FTIR spectra of **1** from Model **1-(III)** calculated using DFT. a) Results from different functionals and basis sets. b) Results for singlet (S=0) and triplet (S=1) spin multiplicities using different functionals and the TZVP basis set.

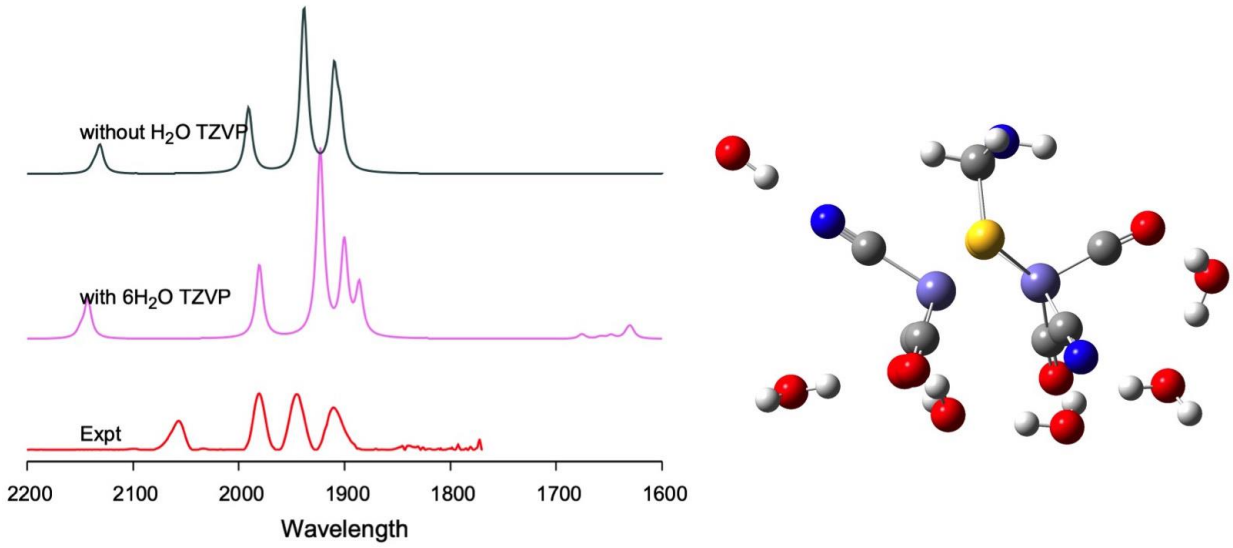

Figure S10. FTIR spectrum and structure of Model **1-(III)** including 6 explicit water molecules calculated using TPSSh/TZVP. The result is compared to a spectrum without explicit water. Colour coding: Fe - purple, Sulfur - yellow, O - red, N - blue, C - grey, hydrogen - white.

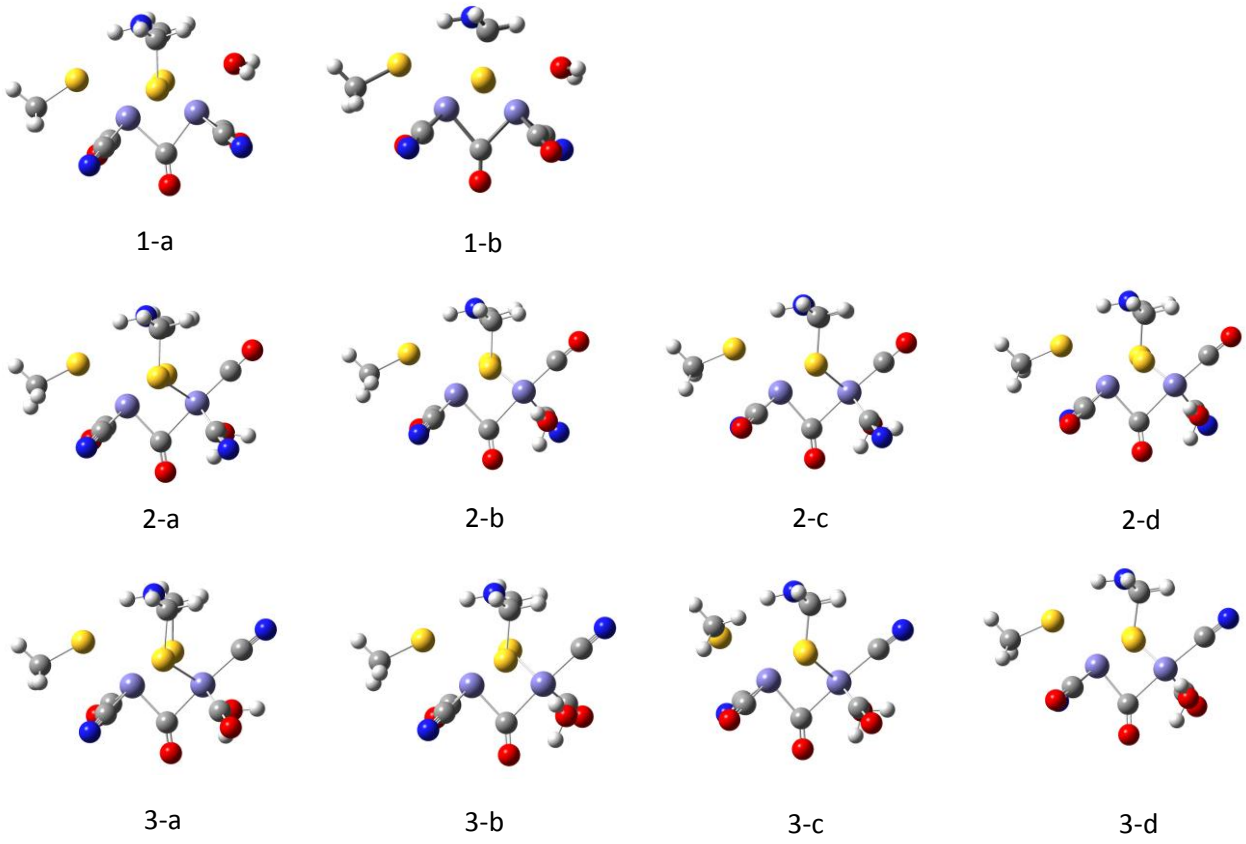

Figure S11. Simplified [2Fe] models of **2** [Fe_2(I,II)(adt)$(CO)_3(CN)_2(H_2O)(CH_3S)$] in different isomers. The isomers are grouped based on the ligand occupying the proposed catalytic site, H_2O, CO or CN. Colour coding: Fe - purple, Sulfur - yellow, O - red, N - blue, C - grey, hydrogen - white.

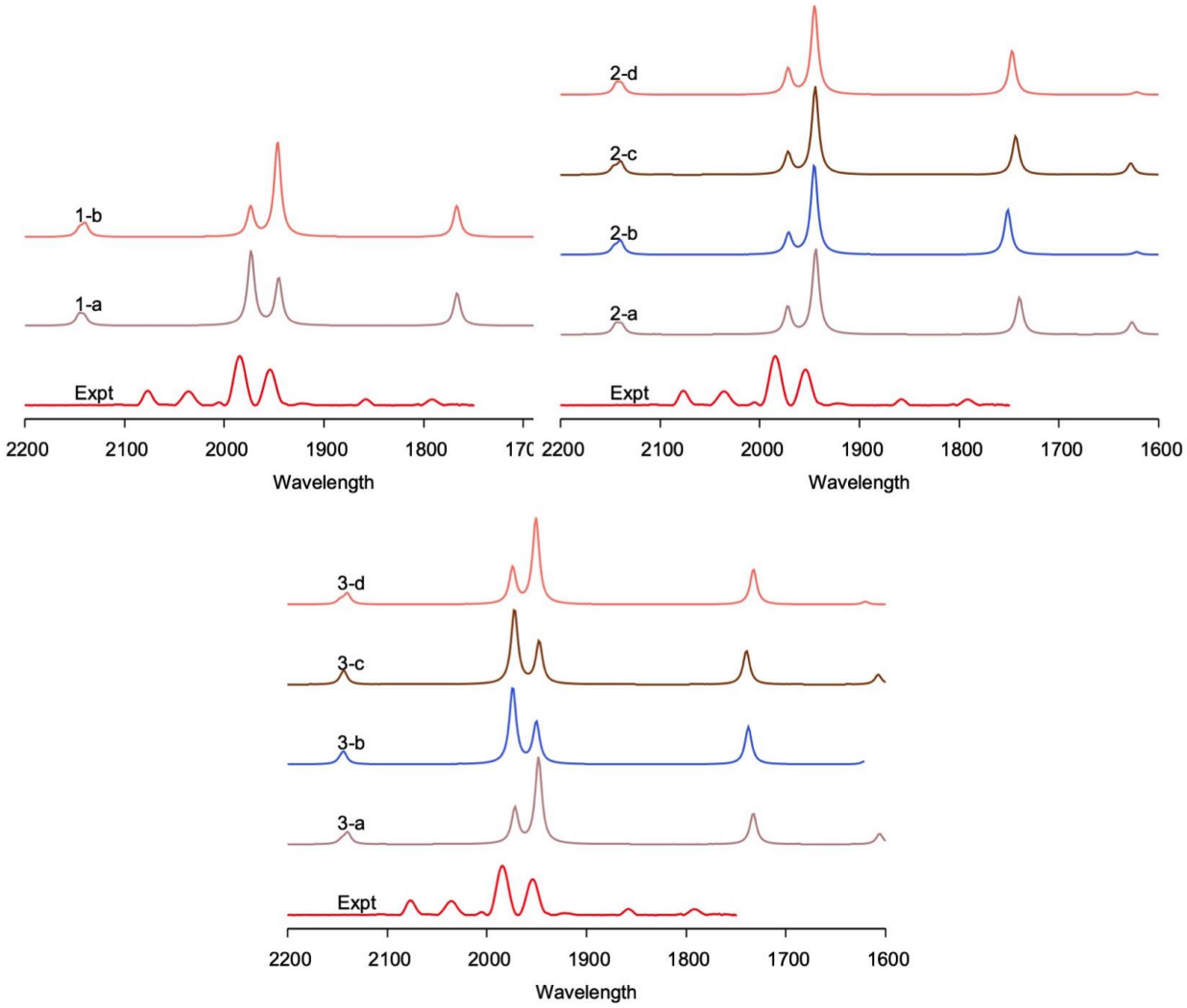

Figure S12. FTIR spectra from simplified [2Fe] models of **2** [Fe_2(I,II)(adt)$(CO)_3(CN)_2(H_2O)(CH_3S)$] in different isomers as shown in Figure S11. Calculations have been performed at the TPSSh/TZVP level of theory.

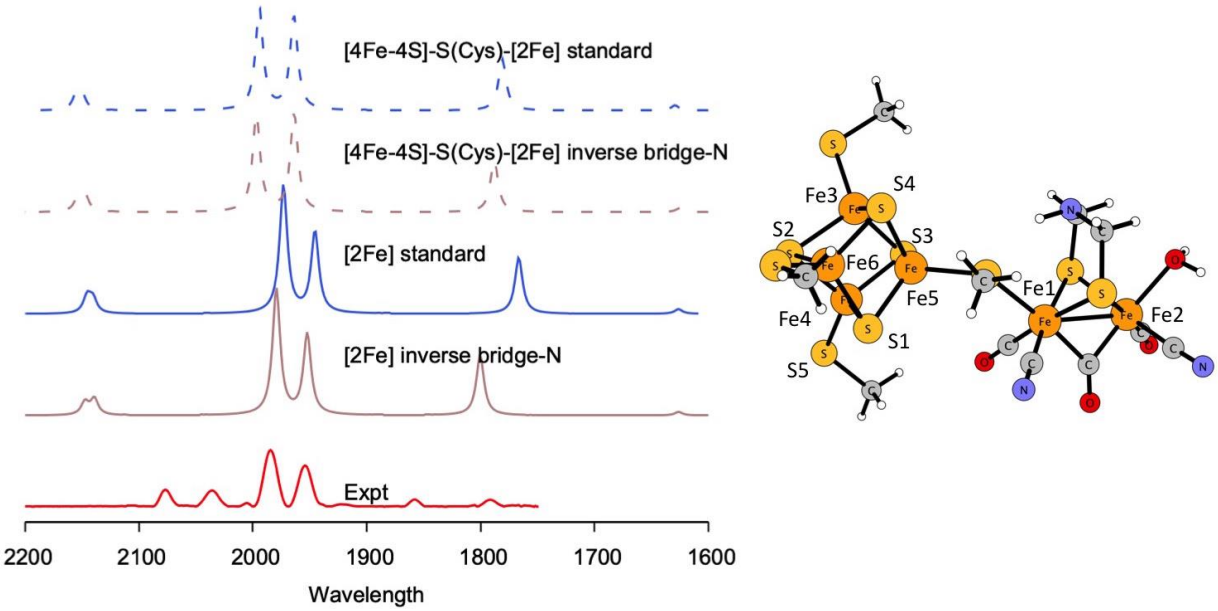

Figure S13. FTIR spectra from [4Fe-4S]-S(Cys)-[2Fe] models of **2-(1-a)** with different orientation of the nitrogen of the bridging adt group calculated using TPSSh/TZVP. The isomer in the picture is labeled as Standard.

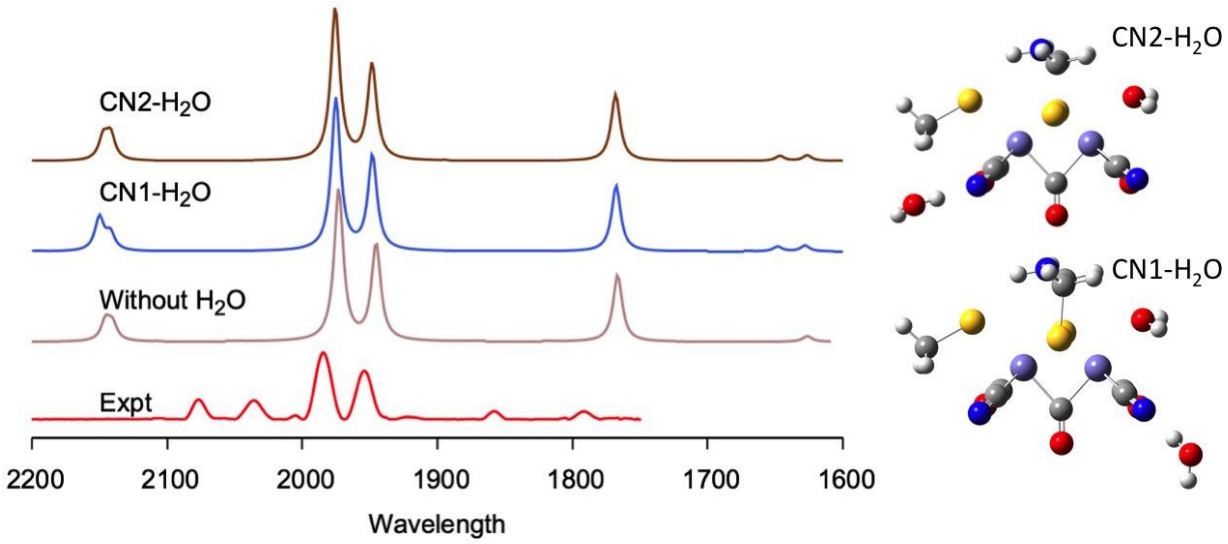

Figure S14. FTIR spectra from simplified [2Fe] model complexes of **2-(1-a)** with and without hydrogen bonding between CN ligands and a single water molecule. Calculations have been performed at the TPSSh/TZVP level of theory. Colour coding: Fe - purple, Sulfur - yellow, O - red, N - blue, C - grey, hydrogen - white.

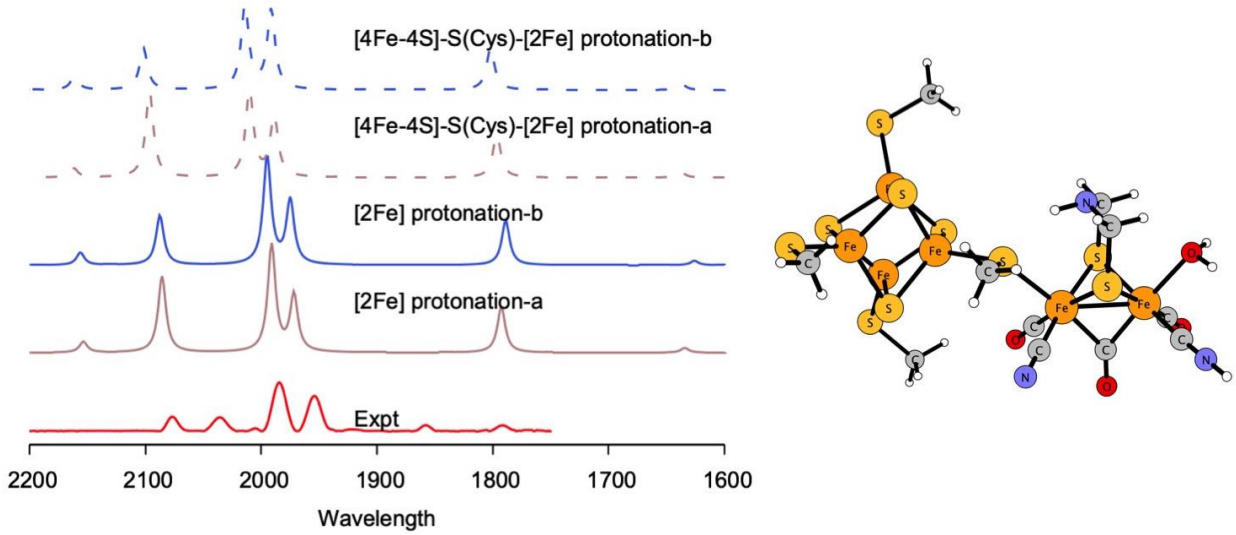

Figure S15. FTIR spectra from [4Fe-4S]-S(Cys)-[2Fe] models of **2-(1-a)** with protonation of a single CN group calculated using TPSSh/TZVP. The isomer in the picture corresponds to protonation of site a.

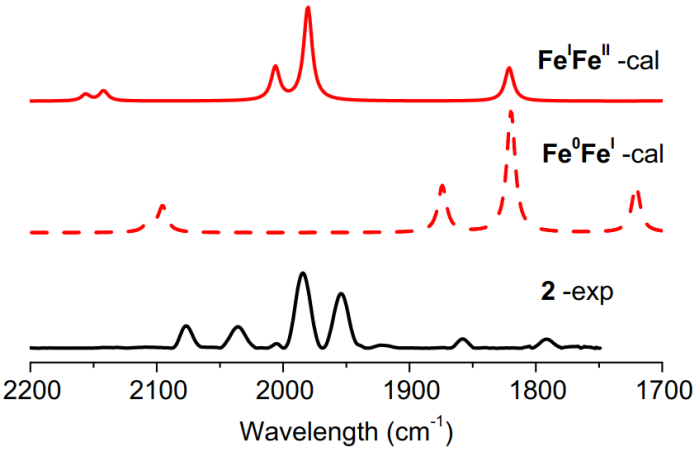

Figure S16. Simulated spectra of **2-(1-b)** in $Fe^{0}Fe^{I}$ and $Fe^{I}Fe^{II}$ oxidation states calculated using TPSSh/TZVP. The $Fe^{0}Fe^{I}$ has been calculated with a protonated bridge as the reduced complex is more likely to be protonated than the oxidized one.

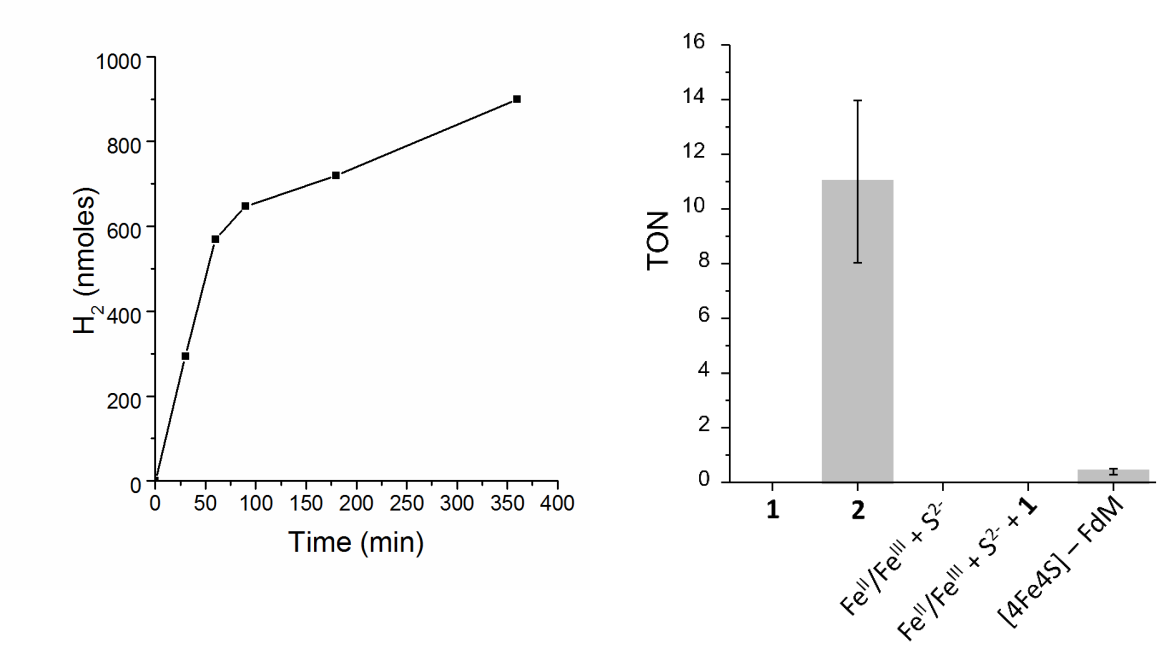

Figure S17. Hydrogen evolution capacity of $[Fe_2(adt)(CO_3)(CN)_2]$-[4Fe4S]-FdM, **2**, compared to relevant control samples (**Left**): H_2 evolution from **2** (52 μM) monitored over 6h. The catalyst shows moderate reactivity for approx. 1h before H_2 evolution slows down. (**Right**): TON for H_2 evolution after 1h for **1** (52 μM); **2** (52 μM); a mixture of Fe^{2+} (104 μM), Fe^{3+} (104 μM) and S^{2-} (208 μM); a mixture of **1** (52 μM), Fe^{2+} (104 μM), Fe^{3+} (104 μM) and S^{2-} (208 μM); [4Fe4S]-FdM (52 μM). Volume of each solution 1.15 mL; TON calculated based on an assumed catalyst concentration of 52 μM (i.e. 60 nmoles).

Assay conditions: aqueous media buffered at pH 8.0 (HEPES 50 mM), methyl viologen (MV^+) 10 mM, 100 mM sodium dithionite.

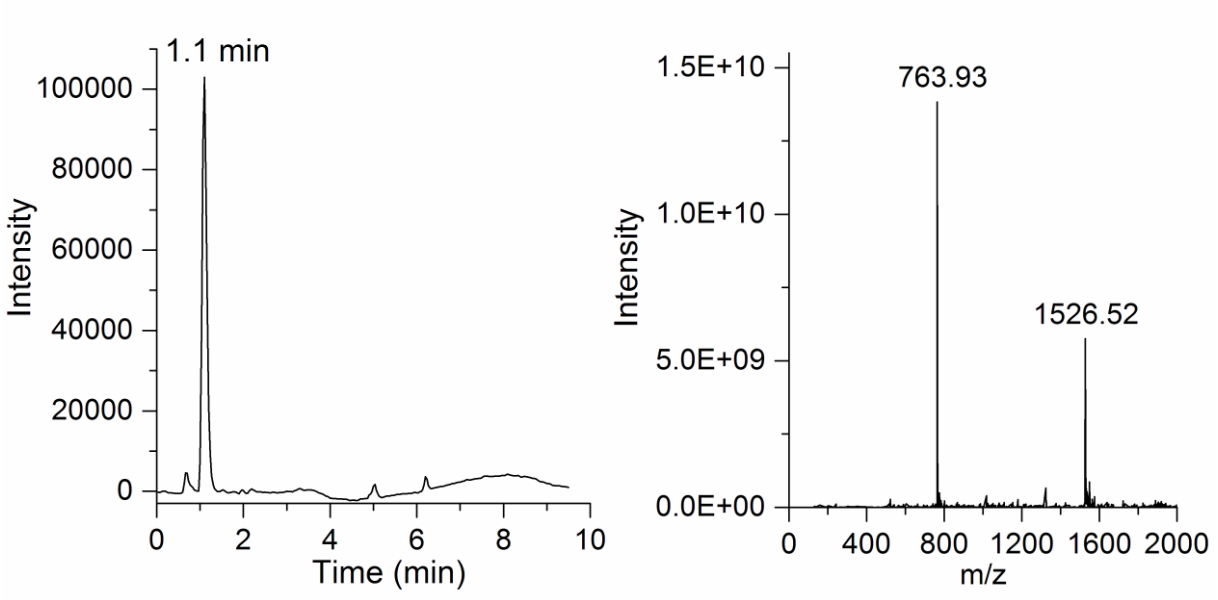

Figure S18. In-house verification of FdM peptide purity by LC-MS. (**Left**): Representative chromatogram of the FdM peptide; (**Right**): Mass spectrum at 1.25 min (expected mass of $[H(FdM)]^+$ = 1526.6). The peptide (0.5 mg) was dissolved in a mixture of CH_3CN/H_2O (22/78, 0.25 mL) containing 0.1 % TFA and injected (5 μL) in an analytical HPLC. Chromatography was performed on a C18-reversed phase silica gel column, using an aqueous–acetonitrile gradient containing 0.05 % (vol/vol) formic acid (1.0 mL/min, gradient: 0.0 min 10% solvent B, 10.0 min 90 % solvent B; solvent A: H_2O; solvent B: CH_3CN , run time = 10 min). The chromatogram was monitored at 220 nm.

Table S1. Comparison between X-ray and TPSSh/TZVP calculated structures for different isomers of $[Fe_2(adt)(CO)_4(CN)_2]^{2-}$. Distances are given in Å and angles in degrees.

	Expt[a]	Expt[b]	Model I	Model II	Model III	Model IV	Model V
Fe(1)-Fe(2)	2.505	2.5090(6)	2.494	2.519	2.504	2.540	2.506
Fe(1)-C(1)	NA	1.940(3)	1.921	1.915	1.913	1.915	1.918
Fe(1)-C(2)	1.797	1.745(3)	1.754	1.759	1.757	1.760	1.758
Fe(1)-C(3)	1.801	1.751(3)	1.754	1.761	1.757	1.759	1.761
Fe(1)-S(1)	2.257	2.2871(9)	2.315	2.295	2.294	2.287	2.293
Fe(1)-S(2)-Fe(2)	67.4	66.49(2)	65.3	66.7	66.0	67.5	65.8

[a] From Wang, Zhen, et al. "Azadithiolates cofactor of the iron-only hydrogenase and its PR 3-monosubstituted derivatives: Synthesis, structure, electrochemistry and protonation." Journal of Organometallic Chemistry 692.24 (2007): 5501-5507.

[b] Structure of 2 in Lawrence, Joshua D., et al. "Diiron Azadithiolates as Models for the Iron-Only Hydrogenase Active Site: Synthesis, Structure, and Stereoelectronics." Angewandte Chemie International Edition 40.9 (2001): 1768-1771.

Table S2. Mulliken spin populations of iron in Model 1-a derived structures in the simplified [2Fe] model and in the full [4Fe-4S]-S(Cys)-[2Fe] model. Standard and inverse refers to the orientation of the nitrogen in the bridging adt ligand. For atom labels, see Figure S13.

Model	Bridge	Fe1	Fe2	Fe3	Fe4	Fe5	Fe6	S1	S2	S3	S4	S5
SImplified	Standard	0.30	0.71	-	-	-	-					
SImplified	Inverse	0.14	0.91	-	-	-	-					
Full	Standard	0.41	0.58	3.45	-3.63	-3.58	3.43	-0.22	-0.12	-0.21	-0.02	-0.14
Full	Inverse	0.28	0.76	3.45	-3.64	-3.58	3.43	-0.22	-0.13	-0.21	-0.02	-0.14

Materials and Methods

Chemicals were purchased from Aldrich Chemicals and used as received, unless otherwise stated. The FdM peptide (NH_2-KL**C**EGG**C**IA**C**GA**C**GGW-$CONH_2$, > 95% purity) was purchased from the Storkbio Ltd Company. The FeS cluster reconstitution yield was influenced by peptide quality, and to minimize the risk of variations between batches the peptides were verified in-house by LC-MS (Figure S18) and UV/Vis. CH_3CN was distilled under N_2 from CaH_2, whereas Et_2O and THF were distilled under N_2 from sodium/benzophenone ketyl. $[Fe_2(adt)(CO)_4(CN)_2](TEA)_2$ (**1**$(TEA)_2$) was synthesized according to literature procedures.[1, 2]

All anaerobic work was performed in an MBRAUN Labmaster glovebox under argon atmosphere ($[O_2] \leq 2$ ppm). UV/Vis spectra were recorded using an AvaSpec Fiber Optic Spectrometer with an AvaLight DHS light source (Avantes). LC-MS was performed on a Dionex Ultimate 3000 HPLC connected to a Finnigan LCQ DECA XP MAX ESI-MS.

Formation of [4Fe4S] – FdM

Assembly of the [4Fe4S] cluster in FdM was performed under strictly anaerobic conditions *via* a modified literature procedure.[3, 4] A 1 mM stock solution of FdM was prepared by dissolving 1.53 mg, 1 μmol of the peptide in 1 mL of HEPES buffer (50 mM, pH 8.0). The stock solution was diluted to a 60 μM final concentration in 1 mL of HEPES buffer (50 mM pH 8.0) with 0.9 % v/v β-mercaptoethanol. After allowing this mixture to stand for 2 h to reduce any disulfide bonds, the following reagents were added from freshly prepared stock solutions (HEPES buffer, 50 mM pH 8.0): $FeCl_3$ (final concentration 120 μM), $FeSO_4{\cdot}(NH_4)_2SO_4{\cdot}6H_2O$) (Mohr's salt) (final concentration 120 μM) and Na_2S (final concentration 240 μM). The resulting yellow-brown reaction mixture was left 2h at room temperature to ensure reaction completion. The formation of [4Fe4S] – FdM was verified by EPR spectroscopy, following reduction of $[4Fe4S]^{2+}$ – FdM to $[4Fe4S]^{+}$ – FdM using dithionite.

Formation of $[Fe_2(adt)(CO_3)(CN)_2]$-[4Fe4S]-FdM (2)

In a standard reaction, a solution of freshly prepared $[4Fe4S]^{2+}$–FdM (60 μM, in HEPES buffer, 50 mM pH 8) was treated with dithionite (1200 μM) to generate $[4Fe4S]^{+}$–FdM, final volume 1 mL. After a 30 min incubation period a 10 μL aqueous stock solution of complex **1** (6 mM) was added (final concentration 60 μM) and the reaction mixture was left at ambient temperature in dimmed light for 30 minutes.

For the non-catalytic H_2 release experiments, the same protocol was followed, but the reaction was performed in a gas tight 8.3 mL vial. H_2 content in the headspace gas was analyzed as described below.

Electron paramagnetic resonance spectroscopy

Measurements were performed on a Bruker ELEXYS E500 spectrometer using an ER049X SuperX microwave bridge, in a Bruker SHQ0601 cavity equipped with an Oxford Instruments continuous flow cryostat, and using an ITC 503 temperature controller (Oxford Instruments). The Xepr software package (Bruker) was used for data acquisition and processing of spectra. Copper standards were prepared at 0.1 mM, 1 mM EDTA and 0.5 mM $CuSO_4$, 5 mM EDTA.

FTIR

IR absorption spectra were recorded on solution samples between 2200 and 1750 cm^{-1} on a Bruker (IFS 66 v/S) spectrometer using a liquid nitrogen cooled MCT detector controlled with OPUS software. All spectra were measured with a resolution of 2 cm^{-1}. The IR measurements were performed with a

demountable FTIR liquid cell (Pike technologies) using CaF_2 windows with 0.025 mm PTFE spacers. The spectra were baseline corrected in OPUS with a concave rubber band correction.

Detection of CO by a hemoglobin-based assay

[4Fe4S]–FdM (from 0.96 to 2.1 μM final concentration) and stoichiometric amounts of complex **1** (0.96 to 2.1 μM final concentration, 1 eq. vs [4Fe4S]–FdM) were incubated for 30 minutes in a sealed cuvette in the presence of sodium dithionite (20 - 40 μM, 20 eq. vs [4Fe4S]–FdM), under strictly anaerobic conditions. In parallel, a stock solution of bovine hemoglobin (SigmaAldrich) in HEPES buffer was reduced to deoxyhemoglobin (HHb, 180 μM) with sodium dithionite (1.80 mM). 50 μL of the HHb solution was then added to the initial reaction mixture with a gas-tight syringe and the absorbance at 419 nm was recorded. The 419 nm wavelength was selected as it represents the maximum of the Soret band characteristic for carboxyhemoglobin (COHb). Concentrations of COHb were calculated using the difference in molar absorption coefficients of HHb and COHb at 419 nm. All samples prepared in HEPES buffer (50 mM, pH 8.0), final volume 1 mL.

Hydrogen production assay and detection

Hydrogen production was determined according to the procedure described by Happe and co-worker for [FeFe] hydrogenase.[5] Under anaerobic conditions, **2** (60 μM, 1 mL) was prepared from freshly reconstituted $[4Fe4S]^{2+}$ – FdM as described above in an 8.3 mL vial. Once the reaction was complete, the vial was sealed (Suba-seal septa, 13, Sigma-Aldrich) and an excess of methyl viologen and dithionite was added (final concentrations: **2** 52 μM, 10 mM methyl viologen and 100 mM sodium dithionite, final volume 1.15 mL). The reaction mixture was then kept at 30 °C, and H_2 production monitored over 6h. Hydrogen production was determined by measuring H_2 content in the headspace gas using a gas chromatograph (PerkinElmer LLC) equipped with a thermal conductivity detector (TCD) and a stainless-steel column packed with molecular sieves (60/80 mesh). The operational temperatures of the injection port, the oven and the detector were 100 °C, 80 °C and 100 °C, respectively. Argon was used as the carrier gas at a flow rate of 35 mL min^{-1}.

Computational results

Geometry optimizations and IR spectra calculations were performed using Gaussian 09 D.01.[6] The solvent was modeled using the polarized continuum model (PCM) with parameters for water. For $[Fe_2(adt)(CO)_4(CN)_2]^{2-}$ (**1**), five structures with different basal/apical alignment of the CN ligands were evaluated, see Figure S7. The main difference is the relative intensity of the CO bands, with a structure with one CN ligand in apical position (**1-iii**) showing the best agreement with experiment, see Figure S8. Varying the density functional (BP86, TPSSh or B3LYP) leads to shifts in absolute frequencies, but have smaller effects on spectral shape than the structural variations, see Figure S9a. Varying the basis set (TZVP or 6-311+G(d,p)) leads to smaller frequency shifts than changes in functional. TPSSh/TZVP leads to good agreement for the CO bond stretches without any shift in the calculated frequencies. The ground state of **1** is a closed-shell singlet and calculations for the triplet structure gives an FTIR spectrum that is not consistent with experiment, see Figure S9b. Compared to the X-ray data, the deviation in the Fe-Fe bond distance is only 0.01 Å and the Fe-C/S bonds are correct within 0.01-0.03 Å. Calculations with six explicit water molecules gave small shifts in the frequency of different peaks, but did not alter the overall spectral shape, see Figure S10.

To model $[Fe_2(I,II)(adt)(CO)_3(CN)_2]$–$[4Fe4S]^{+}$–FdM (**2**), a simplified model complex $[Fe_2(I,II)(adt)(CO)_3(CN)_2(H_2O)(CH_3S)]$ was first designed. Ten different isomers were calculated, see Figure

S11. Three different isomers give the correct relative intensity distribution for the CO peaks, see Figure S12. Out of these three, only **2**-(1-a) leaves the proposed catalytic site with a weakly bound ligand, and this isomer is therefore used in the further modeling. The electronic structure is a mixed-valence Fe(II)-Fe(I) species with Fe spin populations of 0.30 and 0.71 (from left to right in Figure S11).

To improve the description of the 4Fe4S-cluster, calculations were also made with [4Fe-4S]-S(Cys)-[2Fe] models of the active site. The electronic structure of the 4Fe4S cluster shows four high-spin iron centers, with pairwise antiferromagnetic coupling and additional spin on the sulfur atoms. When coupled with the Fe(II)-Fe(I) center, this gives an open-shell singlet state, see Table S2. Including the full model changes the spin density of the two irons by 0.1 and the intensity of the two terminal CO stretches becomes more similar, see Figure S13. However, the overall agreement with experiment is still good.

The main discrepancy between calculated and experimental FTIR spectra is that the split of the two CN bands are underestimated. The effect of an asymmetric hydrogen bonding environments to the two CN groups was tested by including hydrogen bonding from a water molecule. However, this gave only a small split of the CN bands, see Figure S14. Protonating the CN group leads to splits slightly larger than observed in experiment, but the relative intensities are then no longer equal, see Figure S15. The origin of the CN split cannot be conclusively derived from the calculations.

Finally, a comparison between the reduced and oxidized form of **2**, modeled using isomer **2**-(1-b) shows a significant red-shift of the vibrational spectra in the reduced complex, which is not consistent with the changes in the experimental spectrum, see Figure S16.

References

1. H. Li and T. B. Rauchfuss, *J. Am. Chem. Soc.*, 2002, **124**, 726-727.
2. G. Berggren, A. Adamska, C. Lambertz, T. R. Simmons, J. Esselborn, M. Atta, S. Gambarelli, J. M. Mouesca, E. Reijerse, W. Lubitz, T. Happe, V. Artero and M. Fontecave, *Nature*, 2013, **499**, 66-69.
3. S. E. Mulholland, B. R. Gibney, F. Rabanal and P. L. Dutton, *J. Am. Chem. Soc.*, 1998, **120**, 10296-10302.
4. B. R. Gibney, S. E. Mulholland, F. Rabanal and P. L. Dutton, *Proc. Natl. Acad. Sci.*, 1996, **93**, 15041-15046.
5. C. Kamp, A. Silakov, M. Winkler, E. J. Reijerse, W. Lubitz and T. Happe, *Biochimica et Biophysica Acta (BBA) - Bioenergetics*, 2008, **1777**, 410-416.
6. *Gaussian 09, Revision D.01*, M. J. Frisch, G. W. Trucks, H. B. Schlegel, G. E. Scuseria, M. A. Robb, J. R. Cheeseman, G. Scalmani, V. Barone, G. A. Petersson, H. Nakatsuji, X. Li, M. Caricato, A. Marenich, J. Bloino, B. G. Janesko, R. Gomperts, B. Mennucci, H. P. Hratchian, J. V. Ortiz, A. F. Izmaylov, J. L. Sonnenberg, D. Williams-Young, F. Ding, F. Lipparini, F. Egidi, J. Goings, B. Peng, A. Petrone, T. Henderson, D. Ranasinghe, V. G. Zakrzewski, J. Gao, N. Rega, G. Zheng, W. Liang, M. Hada, M. Ehara, K. Toyota, R. Fukuda, J. Hasegawa, M. Ishida, T. Nakajima, Y. Honda, O. Kitao, H. Nakai, T. Vreven, K. Throssell, J. A. Montgomery, Jr., J. E. Peralta, F. Ogliaro, M. Bearpark, J. J. Heyd, E. Brothers, K. N. Kudin, V. N. Staroverov, T. Keith, R. Kobayashi, J. Normand, K. Raghavachari, A. Rendell, J. C. Burant, S. S. Iyengar, J. Tomasi, M. Cossi, J. M. Millam, M. Klene, C. Adamo, R. Cammi, J. W. Ochterski, R. L. Martin, K. Morokuma, O. Farkas, J. B. Foresman, and D. J. Fox, Gaussian, Inc., Wallingford CT, 2013.